Int J Adv Manuf Technol (2017) 92:1113–1125
DOI 10.1007/s00170-017-0192-6

ORIGINAL ARTICLE

The impact of defect morphology, defect size, and SDAS on the HCF response of A356-T6 alloy

A. Ben Ahmed[1] · **A. Nasr**[2] · **A. Bahloul**[3] · **R. Fathallah**[1]

Received: 20 November 2016 / Accepted: 20 February 2017 / Published online: 9 March 2017

Abstract This paper aims to investigate the influence of defect morphology, defect size, and SDAS on the fatigue behavior of A356-T6 aluminum alloy. A 3D finite element analysis for specimens containing different pore morphologies—(i) spherical pore, (ii) elliptical pore, and (iii) complex pore—was implemented. The Chaboche kinematic hardening model embedded in Abaqus is used to characterize the material response during cyclic loading. Kitagawa diagrams for defective A356-T6 are simulated using the defect stress gradient (DSG) approach. A good agreement is found between experimental and numerical results for predicting fatigue limit in the case of spherical defects. The impact of defect morphology on the fatigue resistance is clearly demonstrated. This paper shows that aluminum fatigue resistance is strongly dependent on the defect size, SDAS, and the defect morphology. Therefore, a mathematical model that takes into account the impact of these three parameters is developed using response surface (RS) approach to predict fatigue limit of porous aluminum alloy. Moreover, the effects of defect morphology, defect size, and SDAS on fatigue response and their interactions under fully reserved tensile loading are investigated.

✉ A. Bahloul
bahloulahmad@hotmail.fr

[1] Laboratoire de Mécanique, Matériaux et Procédés (LMMP) , Ecole Nationale d'Ingènieurs de Sousse (ENISO), Université de Sousse, BP 264, Cité Erriadh, 4023 Sousse, Tunisie

[2] Laboratoire de Génie Mécanique (LGM), Institut préparatoire aux études d'ingénieurs de Monastir (IPEM), Université de Monastir, Avenue Ibn Eljazzar, 5019 Monastir, Tunisie

[3] Laboratoire de Mécanique de Sousse (LMS), Ecole Nationale d'Ingènieurs de Sousse (ENISO), Université de Sousse, BP 264, Cité Erriadh, 4023 Sousse, Tunisie

Keywords Fatigue response · A356-T6 alloy · Kitagawa diagram · Multiaxial fatigue behavior · Defect morphology · SDAS · Defect size · Response surface methodology

Nomenclature

E	Young modulus
DSG	Defect stress gradient
a_{∇}	Material parameter describing the defect influence in the DSG criterion
RSM	Response surface methodology
$\sqrt{J_{2,a}}$	Amplitude of the second invariant of the stress tensor [MPa]
R_{σ}	Load ratio
R_m	Ultimate tensile stress [MPa]
α and β	Material constants in Crossland criterion
P_f	Probability of failure
σ_D	Fatigue limit [MPa]
σ_a	Applied load [MPa]
σ_{-1}	Defect free fatigue limit under fully reserved tension loading [MPa]
τ_{-1}	Defect free fatigue limit under fully reserved torsion loading [MPa]
$R_{p0.2\%}$	Yield stress [MPa]
SDAS	Secondary dendrite arming spacing
HCF	High cycle fatigue
R	Defect radius
G_H	Stress gradient
$\overline{\overline{S}}$	Deviatoric stress tensor
$\sqrt{\text{area}}$	Murakami parameter [um]
$\sigma_{\text{Cr},\max}$	The maximum Crossland equivalent stress
$\sigma_{\text{eq},\ \infty}$	The Crossland equivalent stress at infinity
DoE	Design of experiments

1 Introduction

The high mechanical performances of Al-Si cast materials make them very attractive for use especially in automotive and aerospace fields. Since the aluminum mechanical compounds are often subjected to cyclic loads, the Al fatigue behavior has been the subject of various research studies [1–8]. In almost all related researches, fatigue response was shown to be affected by (i) the presiding microstructural parameter (i.e., often characterized by the SDAS (secondary dendrite arm spacing)) and (ii) the casting defects such as shrinkage cavities, gas pores, notches, and oxide films [1–3, 9–14]. Since casting defects are inevitable in the aluminum alloys, many experimental and numerical investigations have been made to characterize their detrimental impact on fatigue properties.

In this context, Ammar et al. [2] investigated the high cycle fatigue behavior of hypo/hyper eutectic aluminum alloys containing various casting defects. The authors showed that the Al resistance is strongly linked to the defect type. In fact, they found that the fatigue rupture is mainly caused by micro surface porosity. More detailed studies conducted later [13–22] showed that the larger the pore is, the more inferior the fatigue limit. It has been found that under a critical pore size (400 ∓ 100 μm), pores have no impact on Al fatigue response and the alloy can be considered as a defect free material. In this case, the SDAS controls the fatigue mechanism and has the major role in the formation of micro-plastic strain and crack initiation. Moreover, experimental studies [7–14] have revealed that the effect of casting porosity on Al high cycle fatigue behavior depends on the load conditions. It was clearly showed that pores have the most pronounced impact for uniaxial loadings comparing to pure torsion fatigue loading. Given that the Al HCF properties are strongly depending on different parameters (SDAS and casting porosity), many researches [18–24] have dealt with the problem of Al fatigue behavior with preexisting pores and aimed to proposed an approach able to predict the endurance limit under multiaxial fatigue loadings.

In this context, Koutiri et al. [21] have experimentally proved that the HCF response of hypo-eutectic cast Al-Si alloy under multiaxial fatigue loadings could not be described by an approach which is written as a linear combination of the hydrostatic stress and the second invariant of the deviatoric stress tensor such as Dang Van criterion.

Later, Roy et al. [20] have made a comparative study to characterize the aluminum fatigue resilience (case of A356-T6) using multiple approaches:

- The Murakami relationship [23]
- The linear elastic fracture mechanics [25]
- The critical distance method (CDM) [26]
- The defect stress gradient (DSG) criterion [27, 28]

They found that both the DSG and the CDM criteria are the most close to the experimental investigations for describing endurance limit under multiaxial fatigue load conditions. Inspired by Roy's work, IbenHouriya et al. [18] proposed a new expression of the DSG criterion by implementing a new parameter that takes into account the SDAS effects. Based on experimental results, they proved that the modified DSG criterion is able to predict adequately the multiaxial high cycle fatigue response of A356-T6 cast alloy containing natural and artificial defects. Recently, Ben Ahmed et al. [29] have developed a probabilistic approach taking into account the dispersion of the secondary dendrite arming spacing (SDAS) for predicting aluminum fatigue limit. In fact, for a given defect, they [29] have transformed the representative loading point in the improved DSG criterion [18] to a scattering surface obtained by random sampling of the SDAS values.

The most previous experimental and numerical investigations [5, 12, 18–22, 24, 29] have defined the pores using the Murakami parameter ($\sqrt{\text{area}}$) [23], and they have often modeled them as spherical or elliptical defects. But, it should be mentioned that experimental studies [19–22, 30, 31] showed that the most dangerous defects on Al-Si fatigue strength have often complex and tortuous morphologies (irregular and branched shapes). However, few works [12, 17] have dealt with the problem of pore morphology's impact on the aluminum fatigue properties.

Hence, one of the aims of this attempt is to evaluate the negative influence of the defect morphology on the Al-Si fatigue strength (case of A356-T6 alloy) by developing a model able to predict the fatigue limit, with considering the effects of the mentioned parameters (SDAS, $\sqrt{\text{area}}$ and defect morphology). Therefore, a 3D finite element model representing porous A356-T6 is proposed. Different defect sizes, different SDAS values, and three defect shapes are considered. The Kitagawa diagrams for the three defect morphologies using DSG criterion are simulated under fully reversed tension loading. Moreover, a comparative study of the resulting diagrams was investigated to highlight the impact of defect morphology. Then, an analytical model taking into account the effects of defect morphology, defect size, and SDAS for predicting fatigue limit of defective A356-T6 aluminum alloy is developed using experiment design approach. The other purpose of this paper is to characterize the correlation between the considered parameters (SDAS, $\sqrt{\text{area}}$ and defect morphology) and to determine their influence on the A356-T6 endurance limit under fully reserved tension loading, using the surface response method.

2 Theoretical background

2.1 Defect stress gradient criterion

Nadot et al. [27] proposed the defect stress gradient (DSG) criterion to caracterize the stress distrubution around a defect and to quantify its impact on the fatigue limit under different loading conditions. The proposed approach is deduced from the Crossland's formulation and it is expressed as follows:

$$\sqrt{J_{2,\ a}} + \alpha P^{*}_{\max} \leq \beta \tag{1}$$

where

$$P^{*}_{\max} = P_{\max}\left(1 - a_d\left(\frac{G_H}{P_{\max}}\right)\right) \tag{2}$$

$\sqrt{J_{2,\ a}}$ is defined as follows:

$$\sqrt{J_{2,a}} = \frac{1}{2\sqrt{2}} \max_{t_i \in T}\left\{\max_{t_i \in T}\sqrt{\left(\overline{\overline{S}}(t_i) - \overline{\overline{S}}(t_i)\right) : \left(\overline{\overline{S}}(t_i) - \overline{\overline{S}}(t_i)\right)}\right\} \tag{3}$$

where $\overline{\overline{S}}$ is the deviatoric stress tensor and G_H is the stress gradiant expressed as follows:

$$G_H = \left(P_{\max}(A) - P_{\max}\left(\sqrt{\text{area}}\right)\right) \Big/ \sqrt{\text{area}} \tag{4}$$

$P_{\max}(A)$ is the the hydrostatic part of stress tensor of the most solicited point on the defect.

$\sqrt{\text{area}}$ is the Murakami parameter.

$P_{\max}(\sqrt{\text{area}})$ is the hydrostatic part of stress tensor for a point located at a distance equal to $\sqrt{\text{area}}$.

a_d, α, and β are three coefficients experimentally identified.

The DSG criterion was modified later by Gadouini et al. [31] then by Vincent et al. [28] using Eshelby's method (Fig. 1). It is expressed as follows:

$$\sigma_{\text{eq}\nabla} = \sigma_{\text{eq,max}} - a\ \frac{\sigma_{\text{eq,max}} - \sigma_{\text{eq},\infty}}{\sqrt{\text{area}}} \leq \beta \tag{5}$$

where

$\sigma_{\text{eq}\nabla}$ The equivalent stress given by the DSG aproach.

$\sigma_{\text{eq , max}}$ The equivalent stress given by HCF criterion in the most sollitated defect zone.

$\sigma_{\text{eq , }\infty}$ The equivalent stress given by HCF criterion far from the defect.

Recently, Iben Houriya et al. [18] improved the DSG criterion by introducing a new parameter (i.e., secondary dendrite arming spacing (SDAS)) describing the microstructure. They used the Crossland criterion to determine the equivalent stress. The new DSG criterion can be expressed by the two following expressions:

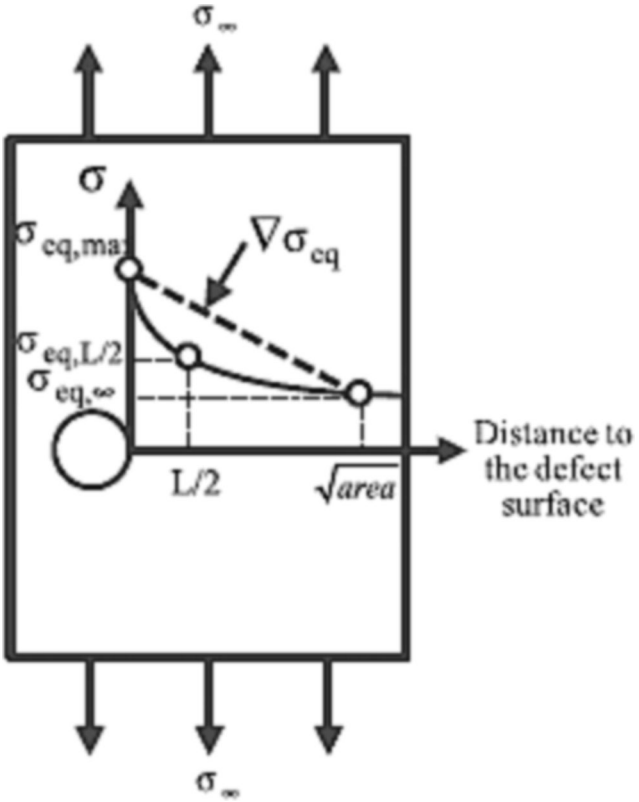

Fig. 1 Principle of DSG approach [24]

(i) For defect free aluminum alloy, fatigue response depends only on microstructure (SDAS) and it can be defined as follows:

$$\sigma_{\text{eq}\nabla M} = \sigma_{\text{Cr,Max}} = \beta_0 \exp\left(-\frac{\lambda_2}{\lambda_0}\right) \tag{6}$$

where λ_2 is the SDAS parameter.

β_0 and λ_0 are two coefficients experimentally identified

(ii) For defective alunimum alloy, fatigue response depends on both SDAS and $\sqrt{\text{area}}$ (defect size) and it can be defined as follows:

$$\sigma_{\text{eq}\nabla M} = \sigma_{\text{Cr,max}} - a_{\nabla}\frac{\sigma_{\text{Cr,max}} - \sigma_{\text{Cr},\infty}}{\sqrt{\text{area}}} \tag{7}$$

Table 1 illustrates the parameters of the modified DSG approach, experimentally identified.

Table 1 Identified parameters of the improved DSG criterion [18]

DSG criterion parameters	Value
β_0	167 (MPa)
α_0	1.8
λ_0	60 (μm)
a_{∇}	470 (μm)

2.2 Overview of response surface methodology

The response surface methodology (RSM) is an optimization tool developed at first by Bucher and Bourgund [32] and improved later by Rajashekhar and Ellingwood [33]. RMS consists in deriving a simple model to linking various process parameters with their response for diverse chosen criteria.

RSM searches the signification of these parameters on the desiring responses [34]. In fact, RMD is an interesting and efficient tool to build an empirical model when the true function linking between the process parameters and the desiring response is very complicated. Since their first use, many of improvement have been introduced to the RSM [35] but the principle steps of this approach that are often employed can be summed up as follows:

(i) Defining the variation range of each input factors
(ii) Preparing the experimental design
(iii) generating the factorial experimental design
(iv) Plotting the surface response
(v) Building the analytical model linking between the process parameters and the desiring response
(vi) Performing additional tests to validate the proposed model

Generally, the mathematical approximating model between the response and their independent input parameters can be expressed as follows:

$$Y = f(X_1, X_2, X_3 \ldots \ldots \ldots X_n) \pm \varepsilon \quad (8)$$

where

Y The designed response.
f The response surface, $X_{i\in[1,n]}$ representing the independent inputs.
ε The error.

In this paper, the response surface method will be used to evaluate the interrelationship between the inputs (SDAS, defect morphology and defect size) and the output (fatigue limit). Therefore, fatigue limit with the corresponding SDAS, defect size and defect morphology are carried out to build the corresponding response surface.

In order to improve the desiring optimum response by taking into account the interaction between different input factors, the fatigue limit will be described by a second order polynomial known as quadratic model which is expressed as follows:

$$f = a_0 + \sum_{i=1}^{n} a_i X_i + \sum_{i=1}^{n} a_{ii} X_i^2 + \sum_{i<j}^{n} a_{ij} X_i X_j + \varepsilon \quad (9)$$

where a_i, a_{ii}, and a_{ij} are respectively the coefficients of the linear effect, quadratic effect, and the interaction between xi and xj. This response surface model is generally collected using the design of experiments (DoE) procedure.

3 Stress determination around the defect

3.1 Finite element modeling

A 3D finite element (FE) simulations using ABAQUS software are carried out to determine fatigue response of A356-T6 aluminum alloy. In order to investigate the influence of defect morphology, three different shapes are considered: (i) spherical defect, (ii) ellipsoidal defect, and (iii) complex defect (Fig. 2).

Concerning the complex defect, it is three-concentric equivalent ellipsoids. It was proposed by Taxer [36] to describe the effects of micro porosity in MAR-M247 alloy. Taxer's researches have demonstrated the efficiency of this model to define cast pores in the material. The FE model using

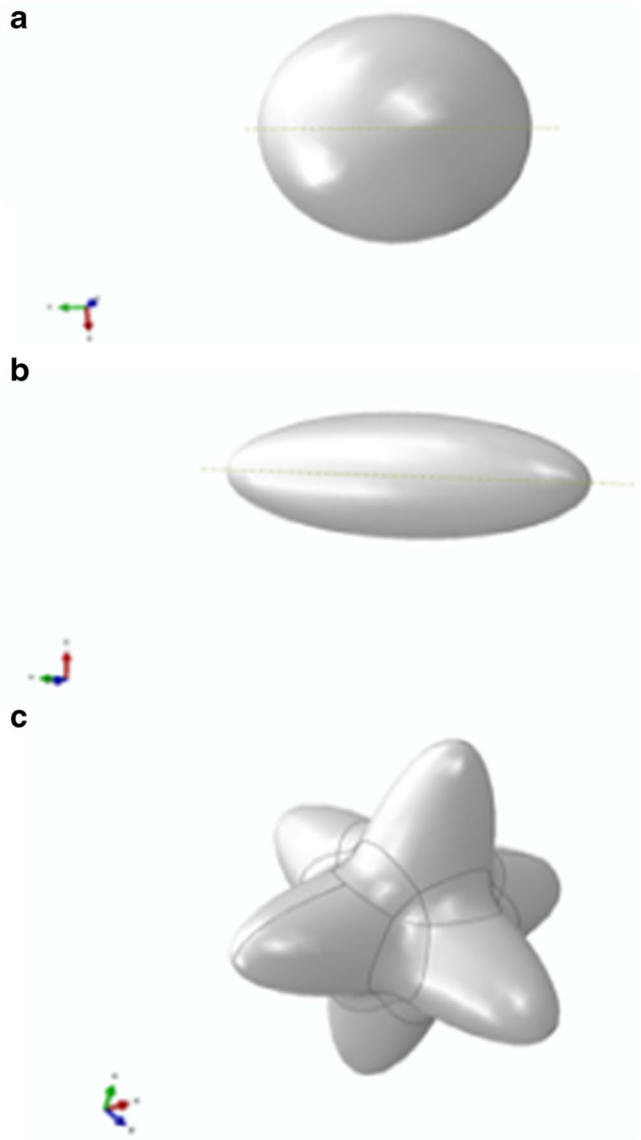

Fig. 2 Representation of the three pore geometries. **a** Spherical pore. **b** Ellipsoidal pore. **c** Complex pore

for this study is inspired from real geometry of experimental tensile test specimen as shown in Fig. 3.

A cylindrical model is used, and owing to the symmetry of the problem, only a quarter of the specimen is modeled. Symmetry and boundary conditions are implemented as illustrated in Fig. 4.

Figure 5 presents the FE-mesh model for the treated specimen in which a very fine mesh is used due to the high strain and stress gradient near the defect surface.

The cyclic behavior of the material is assumed to be elasto-plastic with nonlinear isotropic-kinematic mixed hardening. The Baushinger effect and the mean stress relaxation are taken into account. In the finite element analysis, Chaboche kinematic hardening model is adopted to simulate the A356-T6 alloy response during cyclic loading.

The principal mechanical proprieties for this material are as follows: E (Young modulus) = 70 GPa, ν (Poisson's ratio) = 0.3, $R_{p0.2\%}$ (Yield stress) =200 MPa, R_m (ultimate tensile strength) = 317 MPa, and A (elongation to failure) = 16%. Table 2 sums up the cyclic fatigue parameters for the considered material.

3.2 Stress distribution analysis

Figure 6 illustrates the stress distribution around the three pores under fully reversed tension loading. FE simulations have shown that the plane orthogonal to the applied maximum stress is the highest loaded plane (HLP). Experimental investigations have revealed that cracks propagate in this critical plane [18, 20, 22].

In order to predict the Kitagawa diagrams corresponding to each type of defect, a numerical code is developed within the framework of Python Script. The flowchart of the Python code is present in Fig. 7. For each type of defect morphology, the fatigue limit corresponds to the applied load in which the DSG criterion converges.

4 Experimental design

In this study, experiments were designed based on numerical simulations carried out on defective A356-T6 alloy. The aim of the design matrix (DM) consists in extracting relationships and interactions between the response (fatigue limit under fully reserved tensile) and different input parameters (defect morphology, defect size and SDAS).

In fact, this method helps to investigate both the individual effect of each parameter and describe the interactions between them. The DoE generates 27 experiments with three levels. The obtained results are analyzed using MINITAB 17.0 software. Defect morphology, defect size, and SDAS are chosen as the main independent input parameters in the present work as shown in Table 3. The fatigue limit is considered as an output response which is computed through FE analysis and DSG criterion.

5 Results and discussion

5.1 Validation

This section reports the numerical results carried out to calculate the fatigue response of A356-T6 alloy, having different microstructures and containing spherical defects, using the DSG criterion's new formulation.

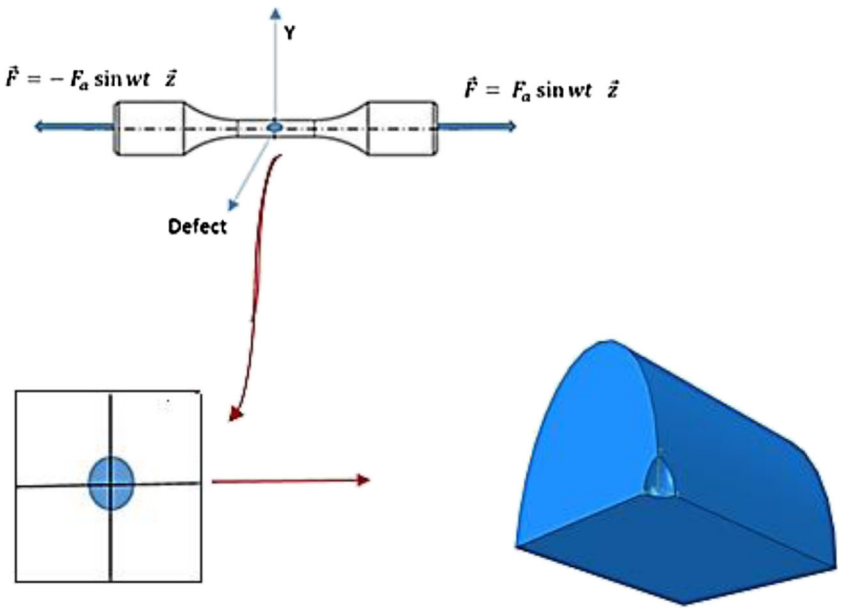

Fig. 3 Experimental specimen and FE model

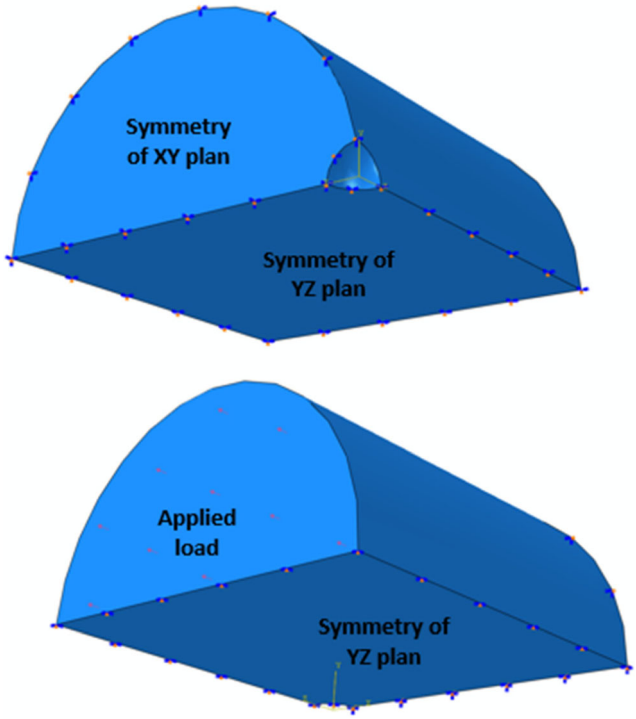

Fig. 4 Boundary conditions and loads applied for FE simulations for tension loading

Table 2 A356-T6 cyclic parameters [37]

Material	E GPa	ν	R_0 MPa	Q	b	C	D
A356-T6	72	0.33	200	30	10	58,000	680

Previous researches [18–20] showed that the critical defect size affecting the A356-T6 fatigue response is around 400 ± 100 μm. Below this value, the alloy is considered as a defect-free material. In this case, the Al HCF behavior is mainly controlled by the microstructure parameter (SDAS). Withal, the experimental data base [18] adopted in this work is conducted for A356-T6 casting alloy with different SDAS values varying from 39.5 to 72 μm. Hence, in the following, the A356-T6 Kitagawa diagrams will be simulated for a defect size range between 500 and 1000 μm and with microstructure parameters corresponding to the upper and lower SDAS values used in the experimental tests [18].

In order to validate the numerical model, Kitagawa diagrams for the fine microstructure (SDAS = 39.5 μ m) and the coarser one (SDAS = 72 μ m) are plotted and compared to the experimental data. Considering the result for fully reserved tension loading presented in Fig. 8, a good agreement between the DSG criterion based on the finite element

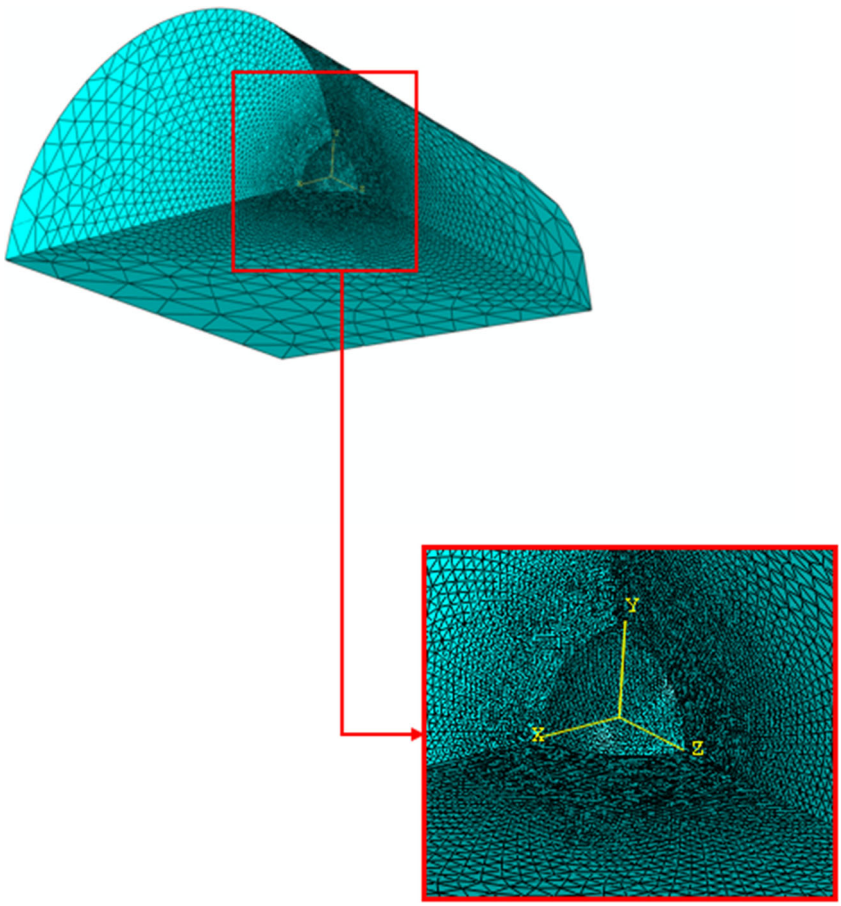

Fig. 5 Mesh refinement around the defect (spherical defect)

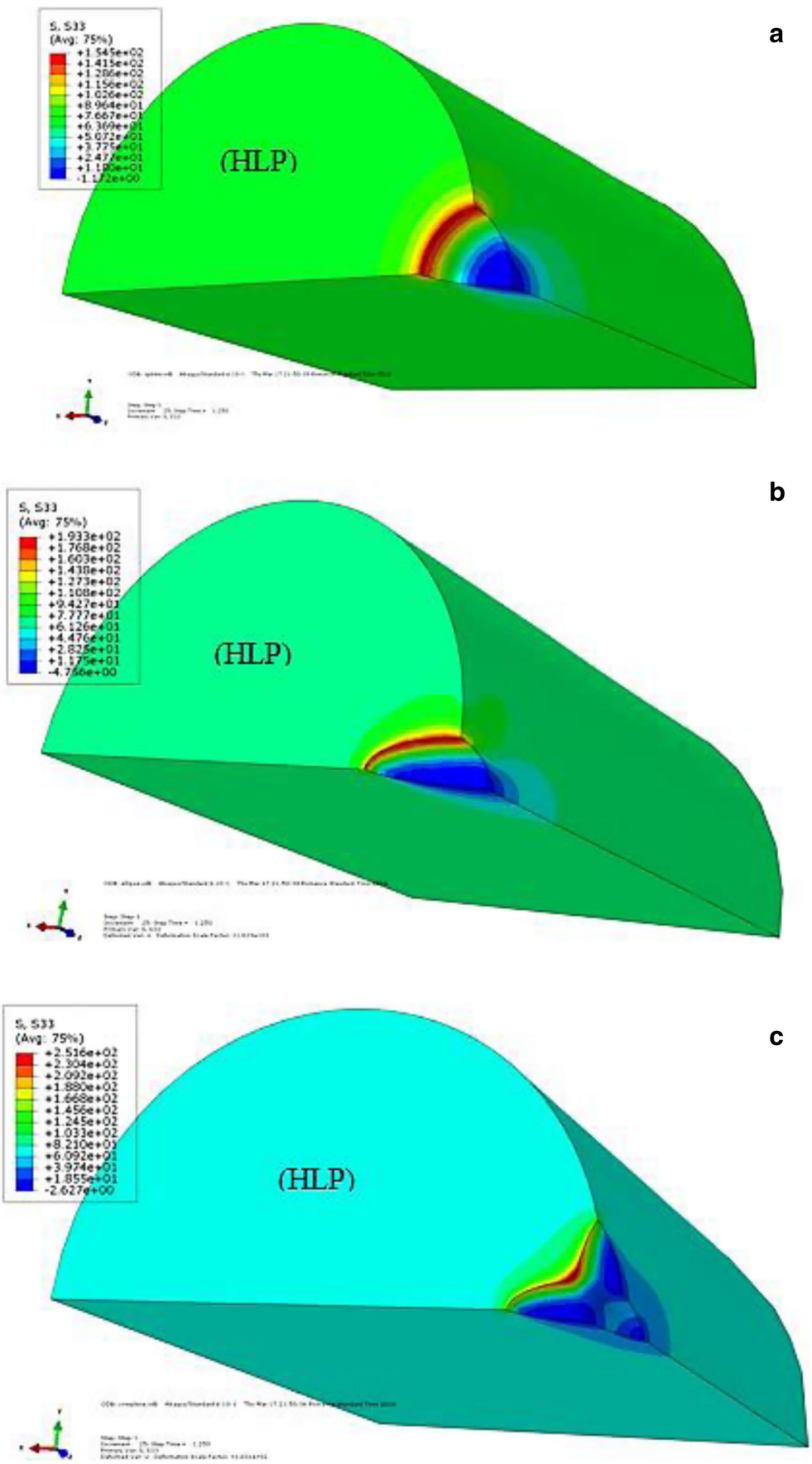

Fig. 6 Stress distrubution in HLP: $\sigma_a = 75$ MPa and $\sqrt{\text{area}}$ = 700 μm.**a** Spherical pore. **b** Ellipsoidal pore. **c** Complex pore

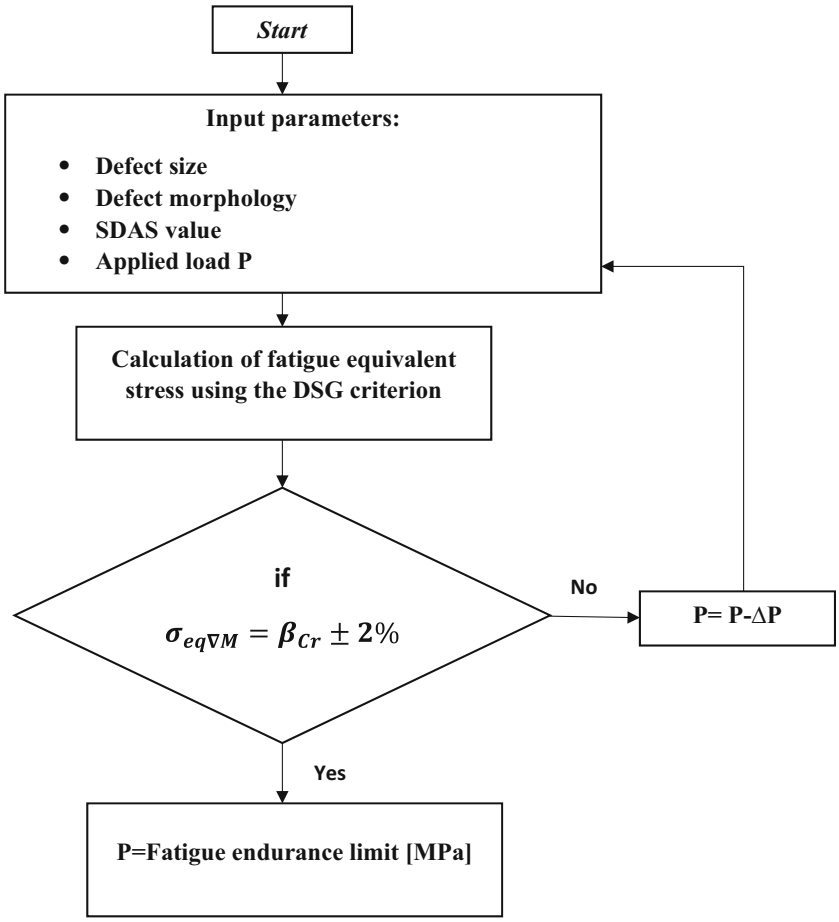

Fig. 7 Flowchart proposed for Kitagawa diagram predictions

analysis and the experimental results is obtained in the case of spherical pore shapes.

In the following part, the DSG criterion will be employed to predict the Kitagawa diagrams for fully reserved tension loading, considering both the defect size (≥500) and the SDAS (39.5 and 72 μm). The generated diagrams are executed in a continuous manner for different defect morphologies (ellipsoidal and complex shapes).

5.2 Morphology effects

In order to highlight the impact of the defect morphology, the Kitagawa diagrams are predicted based on the improved DSG criterion for ellipsoidal and complex pores by following the same procedure used previously.

The generated diagrams are presented in Fig. 9. From the obtained results, it is worth noticing that the A356-T6 fatigue performances vary according to the defect morphology: The more complex the shape, the lower the fatigue limit. In fact, for the same defect size ($\sqrt{area}$) and the same microstructure

Table 3 Experimental parameters and their levels

Parameters	Notation	Level		
		−1	0	1
Defect morphology	A	Spherical	Ellipsoidal	Complex
$\sqrt{area}$ (μm)	B	500	700	900
SDAS (μm)	C	39.5	55.75	72

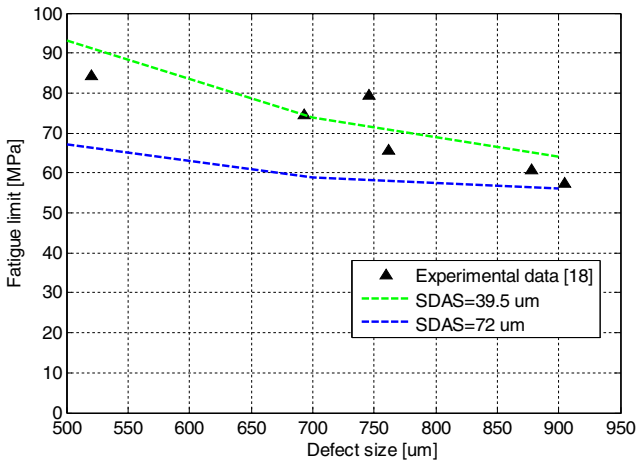

Fig. 8 DSG criteria validation with experimental result for spherical pores

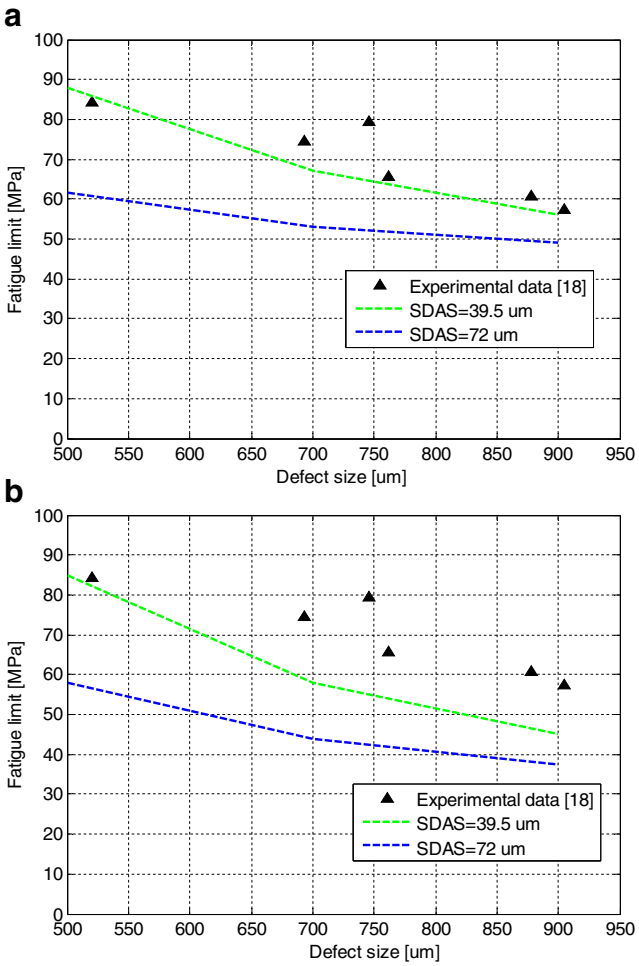

Fig. 9 Kitagawa diagrams for **a** ellipsoidal pores and **b** complex pores

(SDAS), the highest endurance limits are obtained from specimens containing spherical pores and the lowest ones are obtained from specimens containing complex pores. These observations become more pronounced when the defect size decreases. This result is coherent with the experimental investigations [19–22, 29–31] which have revealed that pores with irregular and blanched shapes are acting as stress concentrators in aluminum alloy surface.

Figure 6 shows the stress distribution in the highest loaded plane (HLP) for the three defects, for a defect size ($\sqrt{\text{area}}$) equals to 700 μm and applied load (σ_a) = 75 MPa. It is obvious that the stress distribution varies depending on the considering defect. The complex pores have the highest stress concentration factor (SCF) and the spherical pores have the lowest one. These results demonstrate the notable effect of the morphology on fatigue behavior of A356-T6 alloy. Thus, the defect morphology must not be overlooked in the determination of fatigue response. In the flowing section, an analytical model based on RS method, taking into account the defect morphology, defect size and SDAS, will be proposed.

5.2.1 Development of mathematical model

In the previous section, it was shown that the defect morphology has a significant influence on the fatigue limit. Looking for a model able to predict the fatigue limit of defective A356-T6, considering defect morphology, defect size, and SDAS value, is not yet determined.

In this part, the response surface method coupled with the design of experiment procedure is implemented in order to predict a mathematical model linking the endurance limit of

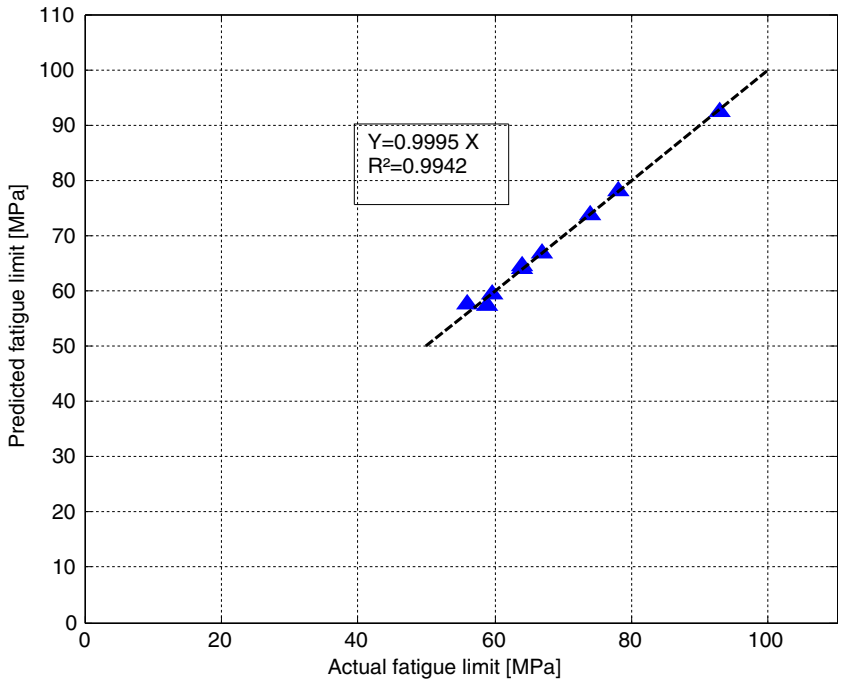

Fig. 10 Model validation for spherical pores

defective A356-T6 as a function of defect morphology, defect size, and SDAS. Therefore, 27 experiments with three levels were generated using Minitab17.0 statistical package, in which the main input factors and their levels in coded and actual values, are summarized in Table 3. The endurance limit is chosen as the main output response. Through using the response surface method, the mathematical model, taking into account the influence of various dominant parameters on the Al 356-T6 fatigue limit is given by the following expression.

$$\begin{aligned}&\text{Fatigue limit} = 57.648-(7.083\mathbf{A})-(11.806\mathbf{B})-(8.056\mathbf{C})-\left(0.694\ \mathbf{A}^2\right)+\left(4.806\ \mathbf{B}^2\right)\\&+\left(1.556\ \mathbf{C}^2\right)-(2.542\ \mathbf{AB})+(0.042\ \mathbf{AC})+(4.750\ \mathbf{BC})\\&R^2 = 99.41\%\end{aligned} \tag{10}$$

In order to ensure the proposed model's performance for describing adequately the fatigue behavior of defective A356-T6 material, the analysis of variance (ANOVA) has been established to justify the goodness of fit of the mathematical model. The R^2 (R^2 = 0.9941) for fatigue limit expression is found to be in reasonable agreement with the adjusted measures. Moreover, a comparison between the experimental results and the response surface model (Eq. 10), in the case of spherical pores, at different SDAS values and defect sizes is performed. The R^2 (R^2 = 0.9942) obtained in Fig. 10 indicates that the RS model is in good agreement with experimental data, providing an accurate and satisfactory results for predicting fatigue limit of cast A356-T6 alloy.

All the above considerations indicate an excellent adequacy of the developed mathematical relationship.

5.2.2 Defect morphology, defect size, and SDAS: effects and interactions

It was shown that defect morphology, defect size and SDAS value are of paramount importance for controlling the fatigue behavior of Al 356-T6 material. In this section, the effect of each factor's level as well as their interactions on the fatigue limit is analyzed based on design of experiments (DoEs) illustrated in Table 4.

Figure 11a shows the main effects of defect morphology, defect size and SDAS value on the fatigue limit. The encoded values (−1, 0, 1), characterizing the level of each factor, is presented on the *x*-axis. The *y*-axis presents the average values of the fatigue limit at a given level. When the line representing the effect of each factor is parallel to the *x*-axis, there is no effect. However, when the line is not parallel to the *x*-axis, a main effect can be always presented and their magnitude depends on the slope of the line. It can clearly be seen that the three parameters have a significant influence in predicting the fatigue limit of defective Al 356-T6 material. In fact, the defect size has the greater impact for controlling the fatigue behavior, followed by the SDAS value and the defect morphology. It is observed that (i) from a range of defect size between 500 and 1000 μm, the fatigue limit average varies from 50 to 75 MPa and (ii) from a range of SDAS value between 39.5 and 72 μm, the fatigue limit average varies from 54 to 70 MPa. According to these results, an important decrease of the endurance limit is observed when the defect size or the SDAS value increase. This observation

Table 4 Design of experiment

Order	Defect morphology	$\sqrt{area}$ (μm)	SDAS (μm)	σ_D (MPa)
1	−1	−1	−1	93
2	−1	−1	0	78
3	−1	−1	1	67
4	−1	0	−1	74
5	−1	0	0	64
6	−1	0	1	59
7	−1	1	−1	64
8	−1	1	0	59.5
9	−1	1	1	56
10	0	−1	−1	88
11	0	−1	0	73
12	0	−1	1	61.5
13	0	0	−1	67
14	0	0	0	57
15	0	0	1	53
16	0	1	−1	56
17	0	1	0	52.5
18	0	1	1	49
19	1	−1	−1	85
20	1	−1	0	70
21	1	−1	1	58
22	1	0	−1	58
23	1	0	0	48
24	1	0	1	44
25	1	1	−1	45
26	1	1	0	41.5
27	1	1	1	37.5

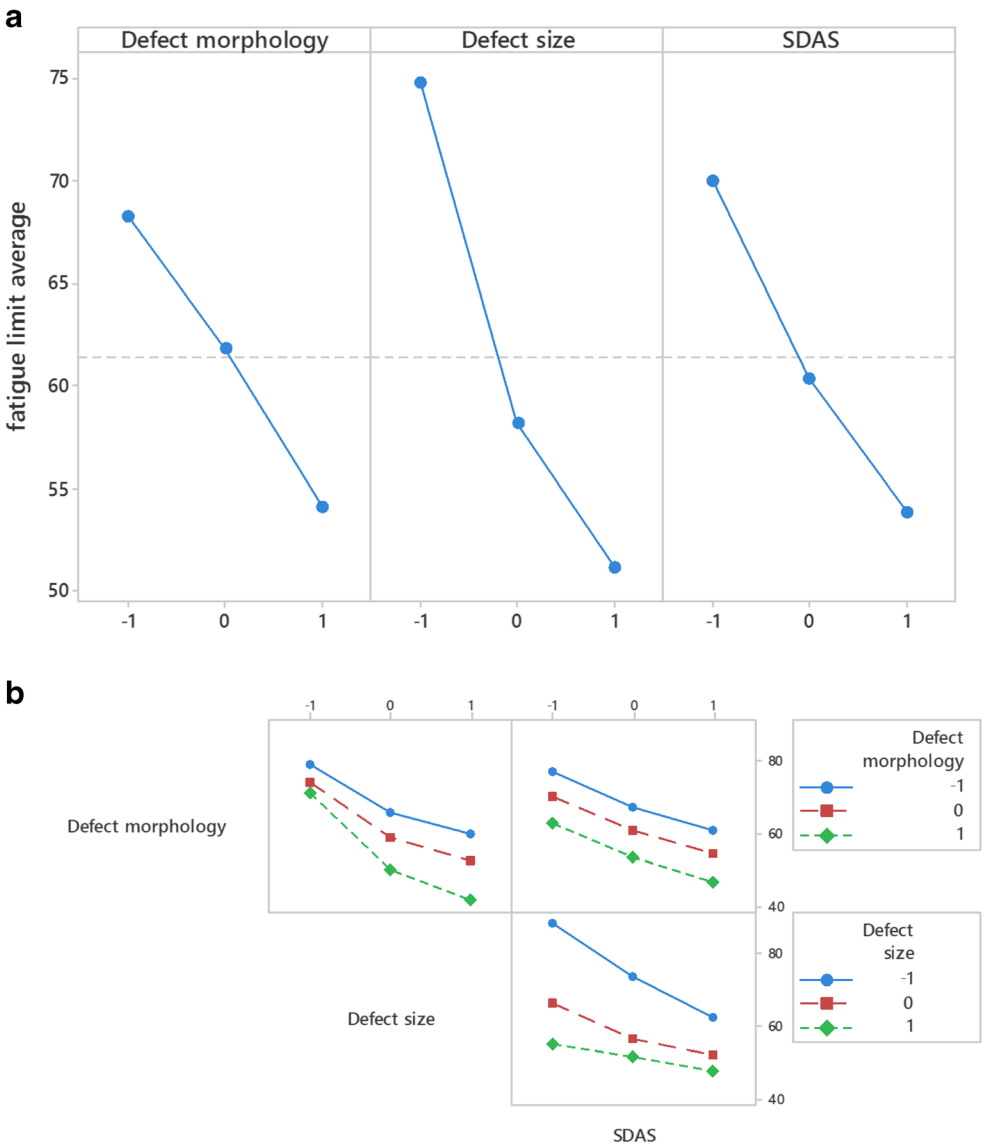

Fig. 11 **a** Effects and **b** interactions of input parameters on fatigue limit

is in good agreement with the experimental studies [18, 20, 22, 24].

Concerning the defect morphology effects, it is observed that the fatigue limit is mostly affected by the complex defect shapes. It is shown that the highest fatigue limit reduction is observed for the specimen containing complex defect and the lowest one is obtained for the specimen containing spherical defect.

Figure 11b presents the interaction plot between the different levels of defect morphology, defect size and SDAS on the fatigue limit response. Parallel lines were observed between the defect morphology and the SDAS parameter. This interaction plot indicates that there is no interaction between these two factors. Moreover, a slight interaction is presented between the defect morphology and SDAS parameters. For defect size equals to 500 μm, an interaction between the defect size and defect morphology was observed.

In order to determine the magnitude and the importance of the effects and the interactions of the considered parameters on the fatigue limit, the Pareto chart is plotted as shown in Fig. 12. As apparent, the defect size, the SDAS, and the defect morphology have a significant influence on the A356-T6 fatigue response with 48.0, 22.4, and 17.3%, respectively. It is clear that the defect size has the greatest impact on it. But, the percentage of 22.4 and 17.3% for the SDAS parameter and the defect morphology, respectively, cannot be neglected.

Hence, the proposed model can be used as an interesting and practical tool to predict the high cycle fatigue behavior of

Fig. 12 Pareto diagram

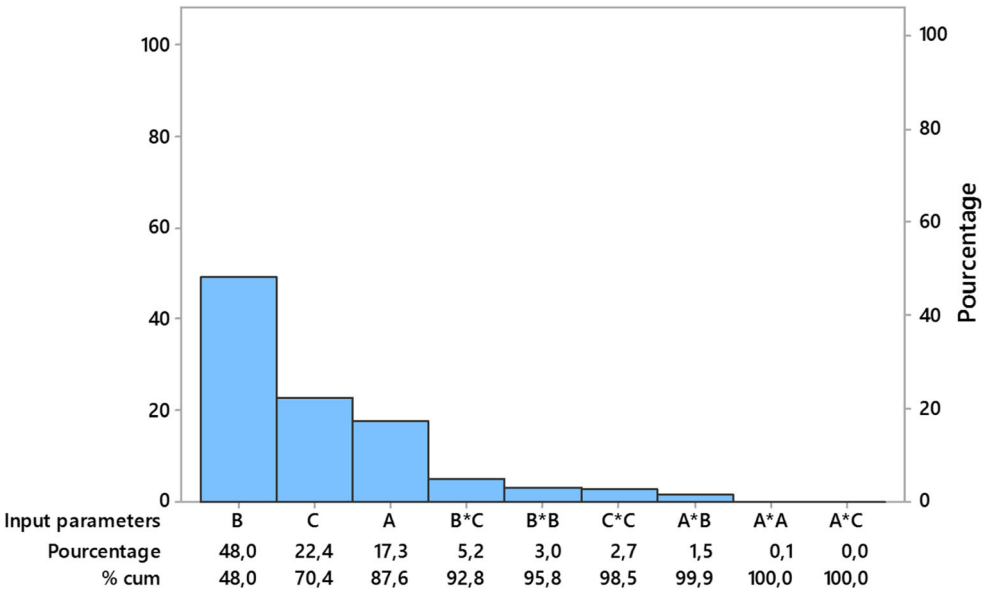

defective A356-T6 alloy. It allows engineers to engaged in practical problem for predicting fatigue limit in a more efficient and reliable way, considering the defect shape, the defect size, and the microstructure heterogeneities.

6 Conclusion

The fatigue strength of A356-T6 aluminum alloy was investigated through a finite element modeling coupled with the defect stress gradient (DSG) criterion. The nonlinear isotropic/kinematic hardening model implemented in ABAQUS software was used to characterize the material's high cycle fatigue behavior under fully reserved tension loading. Attention was focused on confirming the negative influence of the defect morphology on the Al fatigue properties. Therefore, the simulations are carried out for three different defect shapes: spherical, ellipsoidal, and complex. According to the findings, the main conclusions can be summarized as follow:

(i) In the case of spherical defects, numerical results were compared with experiment data showing that the DSG approach gives good predictions (an error that does not exceed 5%).
(ii) It has been shown that the irregular pore shape increases the high stress/strain zone in the vicinity of the surface defect in the Al-Si material. The fatigue resistance is higher for the alloy containing surface spherical pores.
(iii) Numerical results lead to the conclusion that the microstructure (SDAS) and the defect size ($\sqrt{\text{area}}$) are not the only parameters affecting the A356-T6 fatigue performances. The defect morphology must be considered in assessing the aluminum fatigue life.
(iv) Based on the design of experiments (DoEs), a response surface model, able to predict the fatigue limit of defective A356-T6 alloy, is developed. The proposed model can be used as a powerful and practical tool to evaluate the Al high cycle fatigue behavior. In fact, it allows engineers to engaged in practical problem for predicting the endurance limit in a more efficient and reliable way, considering the defect morphology, the defect size, and the microstructure heterogeneities.

References

1. Wang QG, Caceres CH, Griffiths JR (2003) Damage by eutectic particle cracking in aluminum casting alloys A356/A357. Metall Mater Trans A 34A:2901
2. Jordon JB, Horstemeyer MF, Yang N, Major JF, Gall KA, Fan J, McDowell DL (2010) Microstructure inclusion influence on fatigue of a cast A356 aluminum alloy. Metall Mater Trans A 41A:356
3. Wang QG, Praud M, Needleman A, Kim KS, Griffiths JR, Davidson CJ, Caceres CH, Benzarga AA (2010) Size effects in aluminum alloy castings. Acta Mater 58:3006–3013
4. McDowell DL (2007) Simulation-based strategies for microstructure-sensitive fatigue modelling. Mater Sci Eng A 468-470:4–14
5. Borbély A, Mughrabi H, Eisenmeier G, Hoppel HW (2002) A finite element modelling study of strain localization in the vicinity of near surface cavities as a cause of subsurface fatigue crack initiation. Int J Fract 115:227–232
6. Ceschini L, Morri A, Morri A (2014) Estimation of local fatigue behaviour in A356-T6 gravity die cast engine head based on solidification defects content. Int J Cast Met Res 27:1

7. Shaha SK, Czerwinski F, Kasprzak W, Friedman J, Chen DL (2015) Microstructure and mechanical properties of AL-Si cast alloy with additions of Zr-V-Ti. Mater Des 83:801–812
8. Gonzales R, Gonzales A, Talamantes-Silva J, Valtierra S, Mercado-Solis RD, Garza Montes-de-Oca NF, Colas R (2013) Fatigue of an aluminium cast alloy used in the manufacture of automotive engine blocks. Int J Fatigue 54:118–126
9. Ammar HR, Samuel AM, Samuel FH (2008a) Porosity and the fatigue behavior of hypoeutectic and hypereutectic aluminum-silicon casting alloys. Int J Fatigue 30:1024–1035
10. Le V-D, Morel F, Bellett D, Saintier N, Osmond P (2016) Multiaxial high cycle fatigue damage mechanisms associated with the different microstructural heterogeneities of cast aluminum alloys. Mater Sci Eng A 649:426–440
11. Ran G, Zhou J e (2007) Metallographic characterization of porosity in a cast aluminum alloy A356-T6. Mater Sci 546:989–994
12. Xu Z, Wen W, Zhai T (2012) Effects of pore position in depth on stress/strain concentration and fatigue crack initiation. Metall. Mater Trans A 43A:2763
13. Davidson CJ, Griffiths JR, Badiali M, Zanada A (2000) Fatigue properties of a semi-solid cast AL-7Si-0.3Mg-T6 alloy. Metall Sci Technol 18:2
14. Ammar HR, Samuel AM, Samuel FH (2008b) Effect of casting imperfections on the fatigue life of 319-F and A356-T6 Al-Si casting alloys. Mater Sci Eng A 473:65–75
15. Wang QG, Apelian D, Lados DA (2001a) Fatigue behavior of A356-T6 aluminium cast alloys. Part I. Effect of casting defects. J Light Metal 1:73–84
16. Wang QG, Apelian D, Lados DA (2001b) Fatigue behavior of A356-T6 aluminium cast alloys. Part II. Effect of microstructural constituents. J Light Metal 1:85–97
17. Li P, Lee PD, Maijer DM, Lindley TC (2009) Quantification of the interaction within defect populations on fatigue behavior in an aluminum alloy. Acta Mater 57:3539–3548
18. Houriya MI, Nadot Y, Fathallah R, Roy M, Maijer DM (2015) Influence of casting defect and SDAS on the multiaxial fatigue behaviour of A356-T6 alloy including mean stress effect. Int J Fatigue 80:90–102
19. Roy MJ, Yves N, Nadot-Martin C, Bardin P-G, Maijer DM (2011) Multiaxial Kitagawa analysis of A356-T6. Int J Fatigue 33:823–832
20. Roy M, Yves N, Maijer DM, Benoit G (2012) Multiaxial fatigue behaviour of A356-T6. Fatigue Fract Eng Mater Struct 35:1148–1159
21. Koutiri I, Bellett D, Morel F, Augustins L, Adrien J (2013) High cycle fatigue damage mechanisms in cast aluminum subject to complex loads. Int J Fatigue 47:44–57
22. Mu P, Nadot Y, Nadot Martin C, Chabod A, Serrano-Munoz I, Verdu C (2014a) Influence of casting defects on the fatigue behavior of cast aluminum AS7G06-T6. Int J Fatigue 63:97–109
23. Murakami Y (2002) Metal fatigue: effects of small defects and nonmetallic inclusions. Elsevier, Amsterdam
24. Mu P, Nadot Y, Serrano-Munoz I, Chabod A (2014b) Influence of complex defect on cast AS7G06-T6under multiaxial fatigue loading. Eng Fract Mech 123:148–162
25. Rice JR (1988) Elastic fracture mechanics concept for interfacial cracks. J Appl Mech 55:99
26. Susmel L, Taylor D (2008) The theory of critical distances to predict static strength of notched brittle components subjected to mixed-mode loading. Eng Fract Mech 75:534–550
27. Nadot Y, Billaudeau T (2006) Multiaxial fatigue limit criterion for defective materials. Eng Fract Mech 73:112–133
28. Vincent M, Nadot-Martin C, Nadot Y, Dragon A (2014) Fatigue from defect under multiaxial loading: defect stress gradient (DSG) approach using ellipsoidal equivalent inclusion method. Int J Fatigue 59:176–187
29. Ben Ahmed A, Nasr A, Fathallah R (2016) Probabilistic high cycle fatigue behavior prediction of A356-T6 alloy considering the SDAS dispersion. Int J Adv Manuf Technol 0268-3768:1–14
30. Gadouini H, Nadot Y, Rebours C (2008) Influence of mean stress on the multiaxial fatigue behaviour of defective materials. Int J Fatigue 30:1623–1633
31. I. Boromei, L. Ceschini, Al. Morri, An. Morri, G. Nicoletto, E. Riva (2010) Influence of the solidification microstructure and porosity on the fatigue strength of Al-Si-Mg casting alloys. 28–2
32. Bucher CG, Bourgund U (1990) A fast and efficient response surface approach for structural reliability problems. Struct Saf 7(1):57–66
33. Rajashekhar MR, Ellingwood BR (1990) A now look at the response surface approach for reliability analysis. Struct Saf 12(3): 205–220
34. Myers RH, Mongomery DH (1995) Response surface methodology. Wiley, USA
35. Faravelli L (1989) Response-surface approach for reliability analysis. J Eng Mech 115(12):2763–2781
36. Taxer T, Schwarz C, Smarsly W, Werner E (2013) A finite element approach to study the influence of cast pores on the mechanical properties of the Ni-Base alloy MAR-M247. Mater Sci Eng A 575:144–151
37. Le Pen E, Baptiste D (2001) Prediction of the fatigue-damaged behaviour of Al/Al_2O_3 composites by a micro-macro approach. Compos Sci Technol 61:2317–2326